Fast Gate-Based Readout of Silicon Quantum Dots Using Josephson Parametric Amplification

S. Schaal[1,*] I. Ahmed,[2,‡] J. A. Haigh,[3] L. Hutin,[4] B. Bertrand,[4] S. Barraud,[4] M. Vinet,[4] C.-M. Lee,[5] N. Stelmashenko,[5] J. W. A. Robinson,[5] J. Y. Qiu,[6,§] S. Hacohen-Gourgy,[6] I. Siddiqi,[6] M. F. Gonzalez-Zalba,[3] and J. J. L. Morton[1,7,†]

[1]*London Centre for Nanotechnology, University College London, London WC1H 0AH, United Kingdom*
[2]*Cavendish Laboratory, University of Cambridge, J. J. Thomson Avenue, Cambridge CB3 0HE, United Kingdom*
[3]*Hitachi Cambridge Laboratory, J.J. Thomson Avenue, Cambridge CB3 0HE, United Kingdom*
[4]*CEA, LETI, Minatec Campus, F-38054 Grenoble, France*
[5]*Department of Materials Science & Metallurgy, University of Cambridge,*
27 Charles Babbage Road, Cambridge CB3 0FS, United Kingdom
[6]*Quantum Nanoelectronics Laboratory, Department of Physics, University of California, Berkeley California 94720, USA*
[7]*Department of Electronic & Electrical Engineering, University College London, London WC1E 7JE, United Kingdom*

Spins in silicon quantum devices are promising candidates for large-scale quantum computing. Gate-based sensing of spin qubits offers a compact and scalable readout with high fidelity, however, further improvements in sensitivity are required to meet the fidelity thresholds and measurement timescales needed for the implementation of fast feedback in error correction protocols. Here, we combine radio-frequency gate-based sensing at 622 MHz with a Josephson parametric amplifier, that operates in the 500–800 MHz band, to reduce the integration time required to read the state of a silicon double quantum dot formed in a nanowire transistor. Based on our achieved signal-to-noise ratio, we estimate that singlet-triplet single-shot readout with an average fidelity of 99.7% could be performed in 1 μs, well below the requirements for fault-tolerant readout and 30 times faster than without the Josephson parametric amplifier. Additionally, the Josephson parametric amplifier allows operation at a lower radio-frequency power while maintaining identical signal-to-noise ratio. We determine a noise temperature of 200 mK with a contribution from the Josephson parametric amplifier (25%), cryogenic amplifier (25%) and the resonator (50%), showing routes to further increase the readout speed.

Quantum computers require high-fidelity qubit measurement, which must be performed on a timescale faster than the decoherence time to perform quantum error correction [1]. Spin qubits formed in quantum dots (QDs) or donors in silicon are one of the most promising platforms for scalable quantum information processing due to their long coherence times and large integration density [2–7]. When scaling to large arrays of dense qubits [2–4,8] space for additional electrometers and reservoirs, typically required for readout based on spin dependent tunneling [9,10], is limited. Gate-based dispersive rf readout eliminates the need for such additional local structures by embedding the gates that define the QD into a resonant circuit and using Pauli spin blockade [11–17]. Recently, single-shot readout of the singlet-triplet states in a double QD has been demonstrated with gate-based sensors, using a variety of resonator parameters to achieve a range of readout fidelities (for a given integration time): 73% (2.6 ms) [18], 82.9% (300 μs) [19], 98% (6 μs) [20] to 99% (1 ms; using ancillary "sensor" QD and reservoir) [21].

Amplifiers based on Josephson junctions have greatly improved signal-to-noise ratios (SNRs) in the field of superconducting circuits [22–29]. Adopting such approaches in the measurement of QDs at rf or microwave frequencies is expected to lead to corresponding improvements in SNR. This can in principle be achieved at operating frequencies of 4–8 GHz that are typical for Josephson-junction based amplifiers, as demonstrated using an InAs double QD, Josephson parametric amplifier (JPA) and coplanar waveguide resonator [30]. However, lower frequency operation ($\lesssim$1 GHz) becomes necessary [31] for studying lower QD tunneling rates, at which exchange interaction is more easily controlled, and for enabling off-chip resonator fabrication. Suitable amplifiers are available in such a frequency range, for example: a JPA operating at 600 MHz with a noise temperature of $T_{\mathrm{JPA}} = 105$ mK [32] or a superconducting quantum interference device (SQUID) amplifier chain with $T_{\mathrm{SQUID}} = 52$ mK at 538 MHz [33]. Building on such developments, readout of a GaAs based quantum dot at 196 MHz with a noise temperature of 490 mK was recently reported using a SQUID amplifier [34].

In this Letter, we combine rf capacitive gate-based sensing of silicon QDs with Josephson parametric amplification to push the bounds of SNR that can be achieved
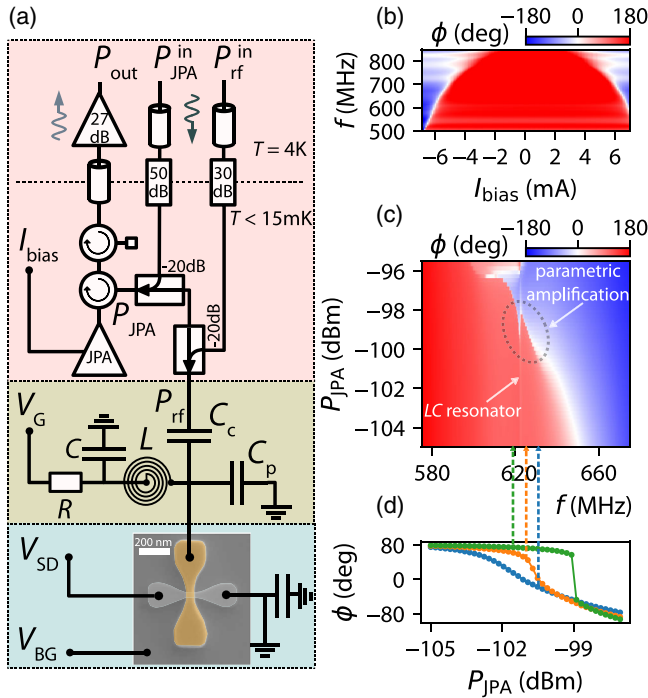
FIG. 1. Setup and Josephson parametric amplifier (JPA). (a) Schematic of the quantum dot readout setup consisting of microwave components (including a JPA), readout resonator, and CMOS quantum dot device (false-colored scanning electron microscope micrograph). (b) Phase response of the JPA as a function of flux bias I_{bias} demonstrating frequency tuning of the JPA. (c) JPA phase response as a function pump power and frequency. The regime of parametric amplification and the readout resonator are indicated. (d) JPA transfer function obtained from linecuts at indicated frequencies in (c). The bistable regime is observed as an abrupt jump in ϕ.

using this technique. We use a well-matched lumped-element high Q resonator containing a NbN spiral inductor and a JPA that operates in the 500–800 MHz band and obtain an overall noise temperature $T_{noise} = 200$ mK at 621.9 MHz. We benchmark the sensitivity of the method using electronic transitions in a silicon multidot devices with large gate coupling (wraparound geometry) fabricated following CMOS processes.

The setup shown in Fig. 1(a) consists of (i) the cryogenic rf delivery and amplification chain including the JPA (pink background); (ii) a lumped-element LC resonator (green); and (iii) the silicon quantum dot device (blue), see [35] for details. The LC resonator is probed using an rf tone with power P_{rf} near resonant frequency f_{rf}. At this frequency, parametric changes in device capacitance ΔC_d due to cyclic single-electron tunneling produce changes in the reflection coefficient $\Delta\Gamma = |(\partial\Gamma/\partial C_d)\Delta C_d|$ [36]. This effect translates into a change in the reflected power with an SNR given by

$$\text{SNR} = |\Delta\Gamma|^2 \frac{P_{rf}}{P_n},$$

where P_n is the noise power.

The optimal SNR is achieved by maximizing $\Delta\Gamma$, maximizing P_{rf} (while remaining below power broadening), and minimizing P_n. $\Delta\Gamma$ is maximized for large loaded quality factor and small parasitic capacitance combined with large gate coupling and a well-matched resonator [37].

The noise power for an amplifier with gain G can be defined as $P_{n,out} = Gk_B(T_{sys} + T_n)B$, where T_{sys} and T_n are the system and amplifier noise temperature (noise added by the amplifier) respectively, k_B is Boltzmann's constant, and B is the amplifier bandwidth. In semiconductor QD measurements, cryogenic high electron mobility transistor (HEMT) amplifiers operating at 4 K typically limit the effective noise temperature (T_{HEMT}) to a few degrees kelvin. By including an additional amplifier (such as a JPA) with gain $G_{JPA}(\gg 1)$ and lower noise temperature (T_{JPA}) at the beginning of the amplification chain, the effective noise temperature T_{noise} can be reduced:

$$T_{noise} = T_{sys} + T_{JPA} + \frac{T_{HEMT}}{G_{JPA}}. \tag{1}$$

For a JPA operating at $T = 10$ mK we expect a minimum of $T_{JPA} = (\hbar\omega/2k_B)\coth(\hbar\omega/2k_BT) = 16.5$ mK.

As shown in Fig. 1(a), the rf signal reflected from the quantum device passes the JPA (which works in reflection) via a circulator and is amplified at 4 K followed by further amplification and quadrature demodulation at room temperature (not shown). Our JPA is a low quality factor ($Q_{JPA} < 100$) superconducting resonator consisting of a SQUID loop array with tunable inductance shunted by a fixed capacitance [38], and is tunable in frequency from 500–800 MHz, as shown in Fig. 1(b), by passing a current I_{bias} through a coil that changes the flux through the nearby SQUIDs. The JPA is pumped via the signal input port and with power P_{JPA}. At low drive power the JPA behaves like a linear resonator, while at high power the nonlinearity of the Josephson junctions manifests in a frequency shift of the JPA to lower frequency until eventually the JPA reaches a bistable regime as shown in Fig. 1(c) [38]. In the regime useful for parametric amplification, the phase of the reflected pump signal varies rapidly with the pump power, as shown in Fig. 1(d), which represents the transfer function of the JPA.

The dynamic range of this JPA is of the order of -130 dBm, making it unsuitable for the signal powers commonly used in previous reflectometry measurements (-90 to -80 dBm) [12]. Here, we overcome this limitation using a high quality factor LC resonator that is well coupled to the input line, achieving a drive amplitude required to obtain a dispersive response at lower input power. The resonator circuit is formed by the parallel combination of a NbN spiral inductor $L = 170$ nH, parasitic capacitance, and the geometric quantum dot device capacitance ($C_p + C_d = 380$ fF), all coupled to the rf line
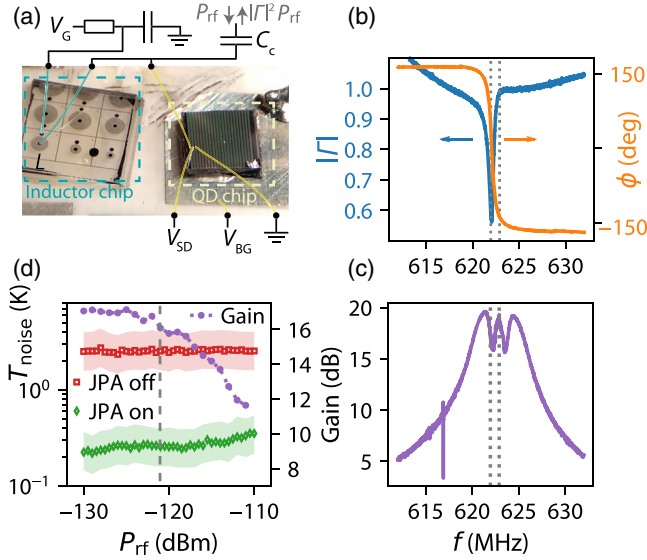
FIG. 2. Characterizing the LC resonator and its operation with the JPA. (a) Shows the resonant circuit, including a schematic of the printed circuit board components and bond wires, the NbN spiral inductor, and the quantum dot device on a separate chip. (b) Magnitude and phase of the reflection coefficient showing the readout resonator ($Q_{\text{load}} = 966$). (c) Gain profile of the JPA when tuned close to the readout resonator frequency (3-dB bandwidth of 6 MHz). (d) JPA gain and estimated system noise temperature at f_{rf} as a function of rf input power showing saturation at high input power (1-dB compression at -121 dBm).

via a coupling capacitor ($C_c = 37$ fF). We observe a resonance in the reflection coefficient $\Gamma = |\Gamma| \exp(i\phi)$ at $f_{\text{rf}} = 1/2\pi\sqrt{L(C_c + C_p + C_d)} = 621.9$ MHz with a loaded quality factor of $Q_{\text{load}} = 966$, impedance $Z = \sqrt{L/(C_p + C_c + C_d)} = 650\ \Omega$, return loss of 3 dB and phase shift $> 180°$ (overcoupled) as shown in Fig. 2(b). When operating at a charge instability in the QD device, the resonator reaches perfect matching. We operate the JPA in phase-preserving mode, where there is an offset $\Delta f = f_{\text{JPA}} - f_{\text{rf}}$ between the JPA pump frequency (f_{JPA}) and f_{rf}, so power from the JPA pump is transferred onto f_{rf} and $f_{\text{JPA}} + \Delta f$ (four-wave mixing) via double-sideband phase modulation as illustrated by the transfer function. We select $\Delta f = 1$ MHz to fall between the bandwidth of the resonator $\Delta f_{\text{rf}}^{\text{3dB}} = 0.65$ MHz and the JPA $\Delta f_{\text{JPA}}^{\text{3dB}} = 6$ MHz. This puts f_{JPA} at the edge of the readout resonator to avoid power broadening due to leakage of the pump signal while maximizing gain at f_{rf}. When tuned and pumped, we achieve a gain of 17 dB at f_{rf} as shown in Fig. 2(c). The decrease in gain near f_{rf} is likely due to large impedance variations of the resonator close to resonance and imperfect matching to 50 Ω.

Figure 2(d) shows the JPA gain and the effective noise temperature close to f_{rf} as a function of P_{rf}. We identify 1-dB compression at -121 dBm. Based on amplifier gain estimations ($G_{\text{HEMT}} = 27 \pm 2$ dB) we obtain an effective

noise temperature $T_{\text{noise}} = 2.5^{+1.4}_{-0.9}$ K with the JPA off and a minimum noise temperature of $T_{\text{noise}} = 200^{+110}_{-73}$ mK based on the SNR improvement with the JPA on. The effective noise temperature with the JPA on increases with increasing power due to saturation. We calculate the contribution of the cryogenic amplifier to T_{noise} [see Eq. (1)] as $T_{\text{HEMT}}/G_{\text{JPA}} = 50^{+28}_{-18}$ mK and estimate T_{JPA} and T_{sys} by comparing T_{noise} when operating the QD device away from or at a charge instability. T_{sys} can have contributions from the resonator circuit (T_{res}) and the QD device (T_{QD}): $T_{\text{sys}} = (1 - |\Gamma|^2)T_{\text{res}} + kT_{\text{QD}}$ [39]. As tunneling between the QD and reservoir occurs adiabatically, no power is dissipated in the device, hence $k = 0$. Based on an increase in T_{noise} of 35^{+24}_{-13} mK when operating at a charge transition (where $|\Gamma|$ decreases from 0.5 to 0), we estimate $T_{\text{JPA}} = 47^{+35}_{-30}$ mK and $T_{\text{res}} = 142^{+94}_{-54}$ mK. We relate T_{res} to thermal noise consistent with typical electron temperatures observed for QDs and we note a JPA efficiency of 36% of the quantum limit (equivalent to ~ 1.5 photons) that is compatible with previous results for operation close to a bifurcation point [27,40,41].

Next, we characterize and compare the improvements in the SNR of gate-based readout using a quantum dot-to-reservoir transition (DRT) in one CMOS silicon nanowire field-effect transistor device and an inter–donor-dot charge transition (IDT) in another device with nominally identical dimensions [16,35,42]. Although we cannot unequivocally determine the nature of the impurity, it presents signatures of a phosphorous atom (see [35] for doping concentration and details on the IDT). QDs form in the corners of the nanowire, as shown in schematic linecuts of the device along the gate and source-drain direction in Figs. 3(a) and 3(b), and have a strong gate coupling $\alpha_{\text{DRT}} = 0.86$, while the donor resides deeper in the channel. When operating at the DRT we observe a signal in the phase as shown in Fig. 3(c) due to a capacitive shift of the resonance corresponding to $\Delta C_d = 0.5$ fF at the maximum. In Fig. 3(d) power broadening of the transition is shown. No broadening occurs for P_{rf} below -120 dBm, while the transition is significantly broadened above -110 dBm. Because of the high Q_{load} of the resonator, only a small input power, compatible with the dynamic range and saturation of the JPA, is required to perform readout and we calculate the rf disturbance at the device gate as $V_{\text{rf}}^{\text{pp}} = [2C_c/(C_c + C_p + C_d)]Q_{\text{load}}V_{\text{in}}^{\text{pp}}$ (e.g., $V_{\text{rf}}^{\text{pp}} = 13\ \mu$V at $P_{\text{rf}} = -130$ dBm).

Next, we use conventional methods to measure the charge sensitivity [35,43] with and without the JPA, which provides a device-specific benchmark on the performance of our gate-based sensor normalized to the gate charge. The SNR as a function of P_{rf}, with and without the JPA, is shown in Fig. 3(e), when operating at a small gate voltage modulation of 50 kHz as indicated in Fig. 3(c). We observe an improvement of up to 8 dB in SNR with the JPA at low rf
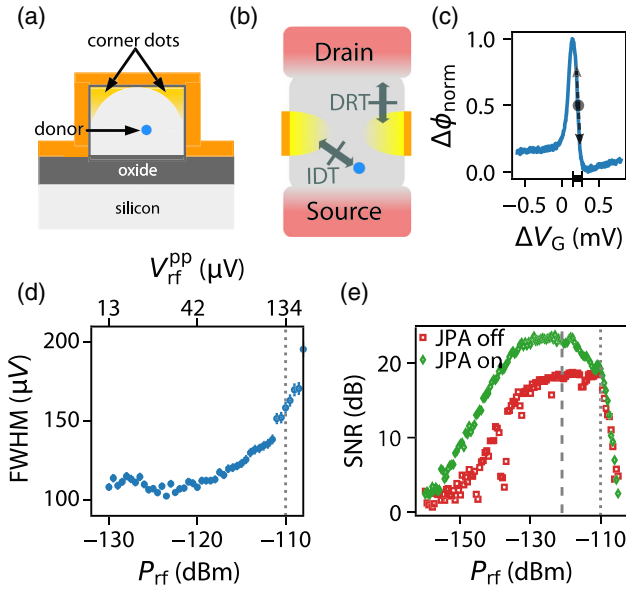
FIG. 3. Dot-to-reservoir transition (DRT) charge sensitivity. (a) Schematic cross section of the QD devices along the gate, and (b) along the source and drain, showing two QDs in the top corners of the nanowire and a donor in the channel. Transitions at which measurements are performed are indicated. (c) Typical phase response across a DRT ($P_{rf} = -125$ dBm). (d) Full width at half maximum (FWHM) of the DRT as a function of power (power broadened at $P_{rf} > 110$ dBm). (e) SNR of the DRT as a function of rf power. The power at which the JPA saturates (dashed line) and significant power broadening occurs (dotted line) is indicated.

FIG. 4. Inter–donor-dot charge transition (IDT). (a) Even-parity IDT between a donor and QD in the device. Electron occupation (N_{dot}, N_{donor}) indicated, up to an arbitrary offset. (b) Normalized phase response along the detuning axis ε in (a) with and without the JPA for two different integration times (traces offset by 1.5 in $\Delta\phi$ for clarity). (c) SNR obtained from traces as shown in (b) as a function of integration time with JPA on and off. Linear extrapolation and SNR = 1 is indicated using dotted lines. (d) Simulated average readout infidelity $1 - F_{avg}$ as a function of τ_{int}. The horizontal dotted line indicates $F_{avg} = 0.997$.

power. Irrespective of whether the JPA is used, for P_{rf} between -130 and -120 dBm the SNR levels off as the DRT begins to become power broadened, and it drops abruptly for powers above -110 dBm. With the JPA on saturation leads to an additional decrease in SNR above -120 dBm. The JPA can either be used to increase the SNR beyond what could otherwise be achieved, and/or to provide the same SNR but at about 10 dB less rf power, with the corresponding reduction in the disturbance of the QD being measured, and its neighbors. When operating well below power broadening ($P_{rf} = -130$ dBm), the charge sensitivity achieved with the JPA is 0.25 $\mu e/\sqrt{\text{Hz}}$ compared to 0.5 $\mu e/\sqrt{\text{Hz}}$ without the JPA, outperforming previous measurements using rf-SET [44] and gate-based approaches [37].

Finally, we estimate spin-readout fidelity using a donor-dot IDT of even parity that exhibits features of spin blockade [14,35]. Figure 4(a) shows the IDT in the normalized phase response as a function of V_G and back-gate voltage (V_{BG}), where the donor transition can be identified due to a stronger coupling to V_{BG}. We determined the effective charge occupation of the donor and QD using the magnetic field response and we calculate a gate coupling $\alpha_{IDT} = 0.36$ and tunnel coupling
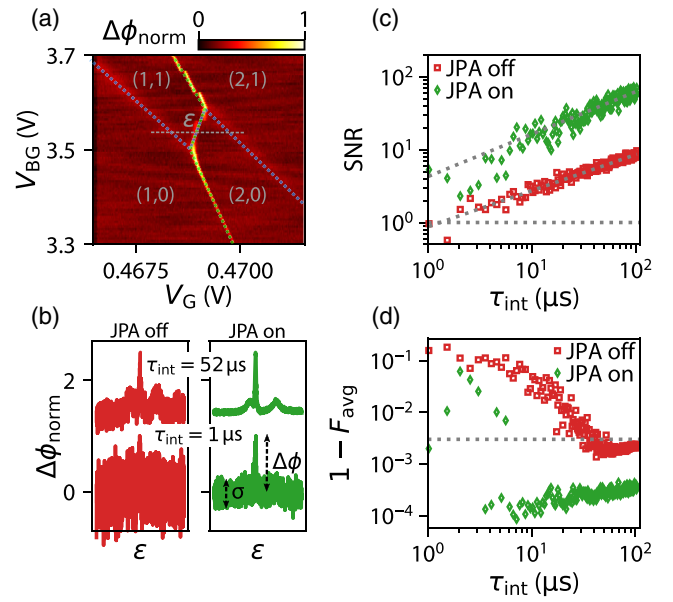
$\Delta_c = 20.9$ μeV, corresponding to a capacitive shift of $\Delta C_d = 0.5$ fF [35]. Figure 4(b) shows an example of the phase response across the IDT, along the detuning axis ε shown in Fig. 4(a) for $\tau_{int} = 1$ μs and $\tau_{int} = 52$ μs. We determine the power SNR from the amplitude $\Delta\phi$ of the IDT signal and the rms amplitude σ of the noise as SNR $= (\Delta\phi^2/\sigma^2)$. Figure 4(c) shows the SNR as a function of integration time with the JPA on and off. Using an extrapolation [dotted lines in Fig. 4(c)] we infer an SNR of unity at $\tau_{int}^{off} = 1.2$ μs and $\tau_{int}^{on} = 80$ ns with the JPA off and on, respectively. However, the limited bandwidth of our resonator prohibits measurements faster than 1.5 μs ($\Delta f_{rf}^{3dB} = 0.65$ MHz). Additionally, we observe that multiple measurements of the SNR with the JPA on for $\tau_{int}^{on} < 10$ μs deviate from the extrapolation, which could be due to noise introduced by the JPA pump signal which is operated only 1 MHz offset the rf signal. Based on the signal and noise levels [as shown in Fig. 4(c)] we simulate the singlet and triplet readout probability densities to obtain a readout fidelity [35,45]. The model includes terms to account for relaxation of the triplet during measurement and we assume $T_1 = 4.5$ ms [18] reported in a similar ^{nat}Si-MOS QD device to demonstrate the improvement in integration time that can be achieved with the JPA. We obtain an average readout infidelity as a function of

integration time which is shown Fig. 4(d) for the JPA off and on. We find that $F_{\text{avg}} > 0.997$ can be reached at a SNR > 5 corresponding to an integration time of at least $\tau_{\text{int}}^{\text{off}} = 32 \ \mu s$ with the JPA off and $\tau_{\text{int}}^{\text{on}} = 1 \ \mu s$ with the JPA on allowing readout faster than the coherence time of electron spins in ^{28}Si ($T_2^* = 120 \ \mu s$ [46]).

We have demonstrated that the SNR of rf gate-based readout of quantum dot devices can be improved using a JPA. We observe a SNR improvement of 8 dB for both dot-to-reservoir and inter–donor-dot transitions when the JPA is operated closed to the rf frequency in phase-preserving mode at 17 dB gain. We have analyzed the performance of the JPA in an external magnetic field, commonly applied in spin qubit devices, and find no disturbance on the JPA performance up to a field of $B_z = 3$ T at the device [35]. The SNR improvement we see is currently limited by the gain of the JPA. Assuming a JPA gain of 23 dB or more, the contribution of the cryogenic amplifier would become negligible. Additionally, the noise added by the JPA can be squeezed below the quantum limit when operating in phase-sensitive mode. Changes in the circuit such as additional isolators between the JPA and readout resonator as well as additional line attenuation and filtering could be beneficial towards achieving larger gain, a lower system noise temperatures and prevent leakage of the JPA pump signal into the readout resonator. In addition, the measurement speed in this implementation is, in principle, limited by the bandwidth of our high-Q readout resonator: increasing the coupling to the line or, preferentially, moving to a higher frequency of the resonator circuit while maintaining high loaded Q should allow submicrosecond fault-tolerant gate-based spin readout. Further development could reduce the footprint of the high Q resonators, to achieve an integrated and scalable readout architecture [47] with the potential of reduced circuit losses and parasitics. Using a traveling wave parametric amplifier with increased bandwidth, frequency multiplexing of multiple resonators could be achieved.

*simon.schaal.15@ucl.ac.uk
†jjl.morton@ucl.ac.uk
‡Present address: Department of Electrical & Electronic Engineering, University of Dhaka, Dhaka 1000, Bangladesh.
§Present address: Massachusetts Institute of Technology, Cambridge, MA 02139, USA.

[1] A. G. Fowler, M. Mariantoni, J. M. Martinis, and A. N. Cleland, Phys. Rev. A **86,** 032324 (2012).

[2] L. M. K. Vandersypen, H. Bluhm, J. S. Clarke, A. S. Dzurak, R. Ishihara, A. Morello, D. J. Reilly, L. R. Schreiber, and M. Veldhorst, npj Quantum Inf. **3,** 34 (2017).

[3] M. Veldhorst, H. G. J. Eenink, C. H. Yang, and A. S. Dzurak, Nat. Commun. **8,** 1766 (2017).

[4] R. Li, L. Petit, D. P. Franke, J. P. Dehollain, J. Helsen, M. Steudtner, N. K. Thomas, Z. R. Yoscovits, K. J. Singh, S. Wehner, L. M. K. Vandersypen, J. S. Clarke, and M. Veldhorst, Sci. Adv. **4,** eaar3960 (2018).

[5] G. Pica, B. W. Lovett, R. N. Bhatt, T. Schenkel, and S. A. Lyon, Phys. Rev. B **93,** 035306 (2016).

[6] C. D. Hill, E. Peretz, S. J. Hile, M. G. House, M. Fuechsle, S. Rogge, M. Y. Simmons, and L. C. L. Hollenberg, Sci. Adv. **1,** e1500707 (2015).

[7] Z. Cai, M. A. Fogarty, S. Schaal, S. Patomäki, S. C. Benjamin, and J. J. L. Morton, Quantum **3,** 212 (2019).

[8] C. Jones, M. A. Fogarty, A. Morello, M. F. Gyure, A. S. Dzurak, and T. D. Ladd, Phys. Rev. X **8,** 021058 (2018).

[9] J. M. Elzerman, R. Hanson, L. H. W. van Beveren, B. Witkamp, L. M. K. Vandersypen, and L. P. Kouwenhoven, Nature (London) **430,** 431 (2004).

[10] A. Morello, J. J. Pla, F. A. Zwanenburg, K. W. Chan, K. Y. Tan, H. Huebl, M. Möttönen, C. D. Nugroho, C. Yang, J. A. van Donkelaar, A. D. C. Alves, D. N. Jamieson, C. C. Escott, L. C. L. Hollenberg, R. G. Clark, and A. S. Dzurak, Nature (London) **467,** 687 (2010).

[11] J. I. Colless, A. C. Mahoney, J. M. Hornibrook, A. C. Doherty, H. Lu, A. C. Gossard, and D. J. Reilly, Phys. Rev. Lett. **110,** 046805 (2013).

[12] M. F. Gonzalez-Zalba, S. Barraud, A. J. Ferguson, and A. C. Betz, Nat. Commun. **6,** 6084 (2015).

[13] K. D. Petersson, C. G. Smith, D. Anderson, P. Atkinson, G. A. C. Jones, and D. A. Ritchie, Nano Lett. **10,** 2789 (2010).

[14] M. D. Schroer, M. Jung, K. D. Petersson, and J. R. Petta, Phys. Rev. Lett. **109,** 166804 (2012).

[15] A. C. Betz, R. Wacquez, M. Vinet, X. Jehl, A. L. Saraiva, M. Sanquer, A. J. Ferguson, and M. F. Gonzalez-Zalba, Nano Lett. **15,** 4622 (2015).

[16] M. Urdampilleta, A. Chatterjee, C. C. Lo, T. Kobayashi, J. Mansir, S. Barraud, A. C. Betz, S. Rogge, M. F. Gonzalez-Zalba, and J. J. L. Morton, Phys. Rev. X **5,** 031024 (2015).

[17] A. Crippa, R. Ezzouch, A. Aprá, A. Amisse, R. Laviéville, L. Hutin, B. Bertrand, M. Vinet, M. Urdampilleta, T. Meunier, M. Sanquer, X. Jehl, R. Maurand, and S. De Franceschi, Nat. Commun. **10,** 2776 (2019).

[18] A. West, B. Hensen, A. Jouan, T. Tanttu, C.-H. Yang, A. Rossi, M. F. Gonzalez-Zalba, F. Hudson, A. Morello, D. J. Reilly, and A. S. Dzurak, Nat. Nanotechnol. **14,** 437 (2019).

[19] P. Pakkiam, A. V. Timofeev, M. G. House, M. R. Hogg, T. Kobayashi, M. Koch, S. Rogge, and M. Y. Simmons, Phys. Rev. X **8,** 041032 (2018).

[20] G. Zheng, N. Samkharadze, M. L. Noordam, N. Kalhor, D. Brousse, A. Sammak, G. Scappucci, and L. M. K. Vandersypen, Nat. Nanotechnol. **14,** 742 (2019).

[21] M. Urdampilleta, D. J. Niegemann, E. Chanrion, B. Jadot, C. Spence, P.-A. Mortemousque, C. Bäuerle, L. Hutin, B. Bertrand, S. Barraud, R. Maurand, M. Sanquer, X. Jehl, S. De Franceschi, M. Vinet, and T. Meunier, Nat. Nanotechnol. **14,** 737 (2019).

[22] D. H. Slichter, C. Müller, R. Vijay, S. J. Weber, A. Blais, and I. Siddiqi, New J. Phys. **18,** 053031 (2016).

[23] R. Vijay, C. Macklin, D. H. Slichter, S. J. Weber, K. W. Murch, R. Naik, A. N. Korotkov, and I. Siddiqi, Nature (London) **490,** 77 (2012).

[24] R. Vijay, D. H. Slichter, and I. Siddiqi, Phys. Rev. Lett. **106,** 110502 (2011).

[25] C. Eichler, C. Lang, J. M. Fink, J. Govenius, S. Filipp, and A. Wallraff, Phys. Rev. Lett. **109,** 240501 (2012).

[26] Y. Chen, D. Sank, P. O'Malley, T. White, R. Barends, B. Chiaro, J. Kelly, E. Lucero, M. Mariantoni, A. Megrant, C. Neill, A. Vainsencher, J. Wenner, Y. Yin, A. N. Cleland, and J. M. Martinis, Appl. Phys. Lett. **101,** 182601 (2012).

[27] M. Hatridge, R. Vijay, D. H. Slichter, J. Clarke, and I. Siddiqi, Phys. Rev. B **83,** 134501 (2011).

[28] N. Bergeal, F. Schackert, M. Metcalfe, R. Vijay, V. E. Manucharyan, L. Frunzio, D. E. Prober, R. J. Schoelkopf, S. M. Girvin, and M. H. Devoret, Nature (London) **465,** 64 (2010).

[29] C. Macklin, K. O'Brien, D. Hover, M. E. Schwartz, V. Bolkhovsky, X. Zhang, W. D. Oliver, and I. Siddiqi, Science **350,** 307 (2015).

[30] J. Stehlik, Y.-Y. Liu, C. M. Quintana, C. Eichler, T. R. Hartke, and J. R. Petta, Phys. Rev. Appl. **4,** 014018 (2015).

[31] Operating at a frequency $f > \Delta_c/4h$ comparable to the tunnel coupling Δ_c results in back-action of the resonator onto the quantum dot device in form of fast voltage oscillations that manifest as Landau-Zener transitions.

[32] S. Simbierowicz, V. Vesterinen, L. Grönberg, J. Lehtinen, M. Prunnila, and J. Hassel, Supercond. Sci. Technol. **31,** 105001 (2018).

[33] M. Mück, J. B. Kycia, and J. Clarke, Appl. Phys. Lett. **78,** 967 (2001).

[34] F. J. Schupp, N. Ares, A. Mavalankar, J. Griffiths, G. A. C. Jones, I. Farrer, D. A. Ritchie, C. G. Smith, G. A. D. Briggs, and E. A. Laird, arXiv:1810.05767.

[35] See Supplemental Material at http://link.aps.org/supplemental/10.1103/PhysRevLett.124.067701 for further details on device fabrication, experimental methods including charge sensitivity fine tuning, the inter-dot transition, JPA performance in an external magnetic field and the readout fidelity model, which includes Refs. [48–51].

[36] R. Mizuta, R. M. Otxoa, A. C. Betz, and M. F. Gonzalez-Zalba, Phys. Rev. B **95,** 045414 (2017).

[37] I. Ahmed, J. A. Haigh, S. Schaal, S. Barraud, Y. Zhu, C. M. Lee, M. Amado, J. W. A. Robinson, A. Rossi, J. J. L. Morton, and M. F. Gonzalez-Zalba, Phys. Rev. Applied **10,** 014018 (2018).

[38] R. Vijay, M. H. Devoret, and I. Siddiqi, Rev. Sci. Instrum. **80,** 111101 (2009).

[39] T. Müller, T. Choi, S. Hellmüller, K. Ensslin, T. Ihn, and S. Schön, Rev. Sci. Instrum. **84,** 083902 (2013).

[40] P. H. Bryant, R. Movshovich, and B. Yurke, Phys. Rev. Lett. **66,** 2641 (1991).

[41] S. Boutin, D. M. Toyli, A. V. Venkatramani, A. W. Eddins, I. Siddiqi, and A. Blais, Phys. Rev. Applied **8,** 054030 (2017).

[42] B. Voisin, V. H. Nguyen, J. Renard, X. Jehl, S. Barraud, F. Triozon, M. Vinet, I. Duchemin, Y. M. Niquet, S. De Franceschi, and M. Sanquer, Nano Lett. **14,** 2094 (2014).

[43] R. J. Schoelkopf, Science **280,** 1238 (1998).

[44] H. Brenning, S. Kafanov, T. Duty, S. Kubatkin, and P. Delsing, J. Appl. Phys. **100,** 114321 (2006), 10.1063/1.2388134.

[45] C. Barthel, D. J. Reilly, C. M. Marcus, M. P. Hanson, and A. C. Gossard, Phys. Rev. Lett. **103,** 160503 (2009).

[46] M. Veldhorst, J. C. C. Hwang, C. H. Yang, A. W. Leenstra, B. de Ronde, J. P. Dehollain, J. T. Muhonen, F. E. Hudson, K. M. Itoh, A. Morello, and A. S. Dzurak, Nat. Nanotechnol. **9,** 981 (2014).

[47] S. Schaal, A. Rossi, V. N. Ciriano-Tejel, T.-Y. Yang, S. Barraud, J. J. L. Morton, and M. F. Gonzalez-Zalba, Nat. Electron. Rev. **2,** 236 (2019).

[48] S. Barraud, R. Lavieville, L. Hutin, H. Bohuslavskyi, M. Vinet, A. Corna, P. Clapera, M. Sanquer, and X. Jehl, Technologies de l'Information et Societe **4,** 10 (2016).

[49] X. Jehl, Y.-M. Niquet, and M. Sanquer, J. Phys. Condensed Matter **28,** 103001 (2016).

[50] K. Y. Tan, K. W. Chan, M. Möttönen, A. Morello, C. Yang, J. Van Donkelaar, A. Alves, J. M. Pirkkalainen, D. N. Jamieson, R. G. Clark, and A. S. Dzurak, Nano Lett. **10,** 11 (2010).

[51] R. Zhao, T. Tanttu, K. Y. Tan, B. Hensen, K. W. Chan, J. C. C. Hwang, R. C. C. Leon, C. H. Yang, W. Gilbert, F. E. Hudson, K. M. Itoh, A. A. Kiselev, T. D. Ladd, A. Morello, A. Laucht, and A. S. Dzurak, Nat. Commun. **10,** 5500 (2019).